



FAULT RUPTURE PROCESS AND INDUCED EARTHQUAKE MOTIONS ON AND NEAR A FAULT BY 3D-FEM ANALYSES

Takayuki MIZUMOTO¹, Toshihiro TSUBOI² and Fusanori MIURA³

SUMMARY

In this study, we performed parametric analyses to examine fault rupture mechanism and induced strong earthquake motions on and near a fault by using three dimensional (3D) finite element method (FEM). First, we compared the magnitude of dislocation for a strike-slip fault obtained by our method with that by Day's method in order to examine the validity of our method. We found that there was a good agreement between the two. Next, by changing the length of dip-slip faults of which the width was kept constant, we performed parametric analyses to investigate the difference of the rupture propagation process, the magnitude of dislocation, the waveforms of acceleration, velocity, and displacement. Finally, we also conducted the simulation by two dimensional (2D) finite element method, and compared the analysis results from 3D-FEM with those from and 2D-FEM to study the similarity and the difference, between the two.

INTRODUCTION

After the 1994 Northridge earthquake, the 1995 Hyogoken-nanbu earthquake, and the 1999 Taiwan Chi-Chi earthquake [1], earthquake engineers recognized the importance of extremely strong earthquake motions and resultant residual large ground deformations on and near the earthquake fault for the earthquake-resistant design [2],[3]. In order to deal with this problem, we have proposed an analysis method to carry out the simulation of the fault rupture process and induced seismic waves simultaneously[4].

Many methods have been proposed to presume the earthquake motion using fault models. The method, however, which can simulate both earthquake motions and induced residual ground displacements simultaneously are limited. We have proposed a method to carry out the simulation of the rupture process of a fault and the corresponding seismic waves simultaneously using a nonlinear finite element method by employing joint elements to model a fault plane [4]. The feature of this technique is to give only the stress-

¹ Doctor Course Student, Yamaguchi University, Graduate School of Science and Engineering, Japan.

Email: mizumoto@earth.csse.yamaguchi-u.ac.jp

² Division of Design, Eirakukaihatsu Co. Ltd, Japan. Email: tsuboi.toshihiro@eirakukaihatu.co.jp

³ Prof. Yamaguchi University, Graduate School of Science and Engineering, Japan.

Email miura@yamaguchi-u.ac.jp

dislocation relationship on a fault plane, and the fault parameters used in the ordinal analysis such as rupture velocity, the magnitude of dislocation, and the source-time function, are obtained as analysis results. The rupture process of a fault, the residual displacement on the ground, and the waveforms of acceleration, velocity, displacement can also be obtained at the same time in our method.

The purpose of this study is to investigate the situation of the rupture propagation, of the magnitude and distribution of the dislocation, of the permanent displacement on the ground surface, and of earthquake motions with the change of the length of the fault and of the direction of the initial stress on the fault plane. First, in order to verify the validity of our method, comparison with the dislocation for a strike slip fault obtained by the method proposed by Day[5] is made. Next, for the dip slip fault, under the condition that the width of the fault was kept constant and the length was changed, we performed the simulation and investigated the difference of the rupture propagation process, the magnitude and the distribution of the dislocation on the fault plane, the distribution of the residual displacement on the ground surface, and the waveform of acceleration, velocity, and displacement. Finally, we compared the results from 3D analyses and those from 2D analyses.

THE ANALYSIS METHOD BY 3D-FEM

Modeling of a fault by 3D joint elements

In this study, a fault is modeled with the arrangement of three dimensional joint elements shown in Figure-1 [6].

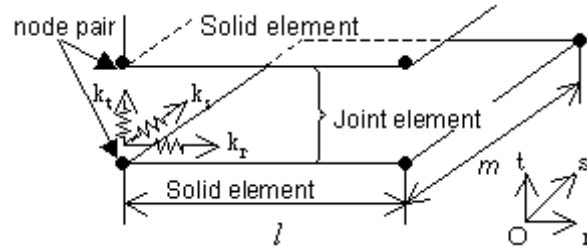


Figure-1 3D-joint element [6]

Each nodal pair is combined by the joint springs in three directions, i.e., k_r , k_s and k_t . The stiffness matrix $[K]_j$ of this joint element is given by the following equation.

$$[K]_j = \begin{bmatrix} [E]_j & -[E]_j \\ -[E]_j & [E]_j \end{bmatrix} \quad (1)$$

The submatrix $[E]_j$ is a diagonal matrix in which the diagonal elements are given by the following equation.

$$diag([E]_j) = \frac{lm}{4} (k_r, k_s, k_t, k_r, k_s, k_t, k_r, k_s, k_t, k_r, k_s, k_t) \quad (2)$$

Where, l and m are the length of the two sides of a joint element (see Figure-1). The relationship of shear stress of the fault plane and relative displacement i.e., dislocation, ε_o , is shown in Figure-2. A 3D joint element has shear stresses τ_r and τ_s in r and s direction. Therefore, the resultant shear stress, τ , and relative displacement, ε_o , shown in Figure-2 is expressed by the following equations (3), and (4).

$$\tau = \sqrt{\tau_r^2 + \tau_s^2} \quad (3)$$

$$\varepsilon_o = \sqrt{u_r^2 + u_s^2} \quad (4)$$

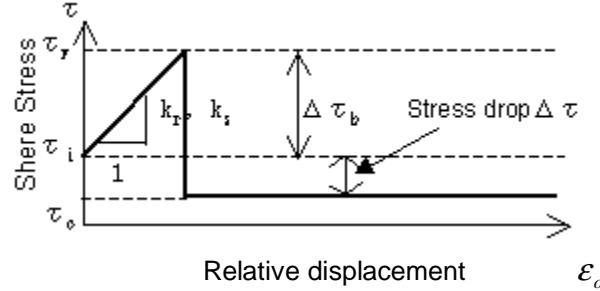


Figure-2 Constitutive relationship

Where, u_r and u_s are the relatively displacements in r and s directions. When the shear stress τ reaches the yield shear stress τ_y , stress drop, $\tau_y - \tau_o$, occurs and initiates sliding at the moment. Where, τ_o is the residual stress. The stress drop is divided into two components in the directions of r and s in proportion to the magnitude of the shear stress components at that time.

Equation of motion

The crust is modeled with 8 node isoparametric elements, and a fault plane is modeled with joint elements, as described above. The viscous boundary is introduced on the artificial outside boundary of the model to reduce the influence of the reflecting wave [7]. The equation of motion which includes the viscous boundary is given by the following equation.

$$[M]\{\ddot{u}\}_n + ([C] + [CV])\{\dot{u}\}_n + [K]\{u\}_n = \{F(n, s)\} \quad (5)$$

Where, [M] is the mass, [C] is the damping, [K] is the stiffness matrices, respectively. [CV] is a viscous boundary matrix including the front, rear, left, right, and bottom boundaries of the model. $\{u\}_n$ is a nodal displacement vector at the time $t = n \times \Delta t$. Where “n” is the number of steps, Δt is a time interval. The symbol, $\dot{\bullet}$, represents the time differentiation and “s” of the external force vector $\{F(n, s)\}$ stands for the nodal pair where stress drop occurs at n time step.

Since the equation of motion has the nonlinear nature as shown in Figure-2, the load transfer method is employed to solve the nonlinear equation. The calculation method is the same as already explained for a 2D problem in the reference [4] in detail.

ANALYSIS MODEL

3D analysis models

Table-1 lists the analysis cases and corresponding fault parameters of the 3D models. Direction of the initial stress, λ , shown in Figure-4, means the angle which the direction of initial stress makes with the Y-axis.

Table-1 Analysis cases and corresponding fault parameters

Case	Width(km)	Length(km)	Angle of tilt(°)	Stress drop(MPa)	Direction of initial stress(°)
1	15	16	90	3.5	90
2	15	22	90	3.5	90
3	15	30	90	3.5	90
4	15	45	90	3.5	90

Figure-3 shows the 3D analysis model (27552 nodes, number of freedom : 82656). The model is for case3 and the size is 30km (X direction) in horizontal direction, 40km (the direction of Y) in perpendicular direction, and 20km in vertical direction (the direction of Z), in the shape of rectangular parallelepiped. The isoparametric element which models the crust is a 1km cube. A fault plane is included in the plane represented by the thick line, i.e., the quadrilateral EFHI. The rectangular slashed zone is equivalent to a 2D analysis model, and the fault in this case, i.e., 2D analysis, is expressed by a straight line AG. The properties of the crust are; shear wave velocity is 4000 m/s, unit weight is 24.5 kN/m³, the poisson's ratio is 0.25, and damping factor is 2%.

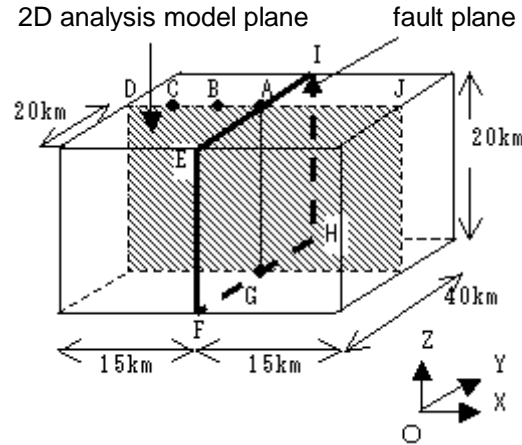


Figure-3 3D analysis model

The plane EFHI (Y-Z plane) which includes a fault plane is shown in Figure-4. The bottom and both side ends of this plane, i.e., the gray zone in Figure-4, are assumed to be non-rupturing zone, and very large value is given to τ_y of the joint element in this zone. The hypocenter is expressed by the symbol of ■ in Figure-4. The initial stress τ_i of the joint elements of the hypocenter is set to be slightly larger than τ_y . The location of the hypocenter is assumed to be the central deepest part of the fault plane by referring the earthquakes in which the rupture propagated to the upper part from the deep part of the fault plane, such as the Northridge earthquake [8] and the Chi-Chi earthquake [1]. The residual shear stress, τ_o , of 1.0MPa (10bar) and the yield shear stress, τ_y , of 9.5MPa were given to all joint elements, and the distribution of the initial stress, τ_i , was given as shown in Figure-5 with the average stress drop of 3.5MPa (35bar). This distribution was determined so that the rupture velocity was about 0.9 times the shear wave velocity.

The stress drop of past earthquakes is within the range between about 1.0 MPa and 10.0MPa. Therefore, the stress drop was set to be 3.5MPa. The spring constant of the joint elements, k_r , k_s , k_t , were set to be $1.02 \times 10^7 \text{ N/m}^3$ based on the pre-parametric analysis on the effect of the magnitude of the joint springs on the fault rupture process and corresponding seismic waves.

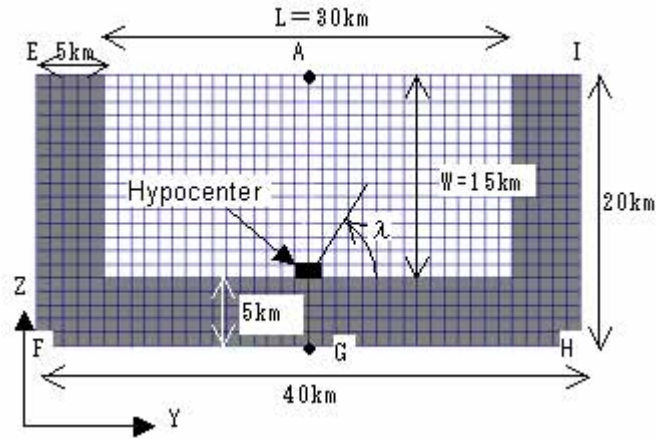


Figure-4 Fault plane (case3)

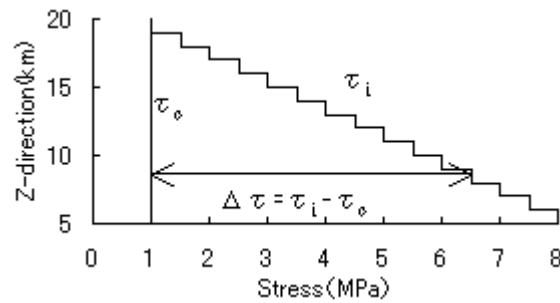


Figure-5 Distribution of the initial stress τ_i and the residual stress τ_o

The width of the non-rupturing zone illustrated in Figure-4 is 5km, that is, the magnitude of the fault plane in case3 is 15km in width and 30km in length.

2D analysis model

Figure-6 shows the 2D analysis model (672 nodes, number of freedom : 1344) for comparing with 3D analysis results. This model is 20km (Z direction) deep, and 30km (X direction) long according to the 3D model. The size of a mesh is 1km in square. The distribution of τ_o , τ_y , τ_i , fault width of 15km, stress drop of 3.5MPa, the spring constants k_r , k_s , and k_t , shear wave velocity, unit weight, and the poisson's ratio are the same as those of 3D analyses. However, since it is 2D analysis, the length of the fault is infinite in Y direction. The central thick line is the fault and ■ is the hypocenter.

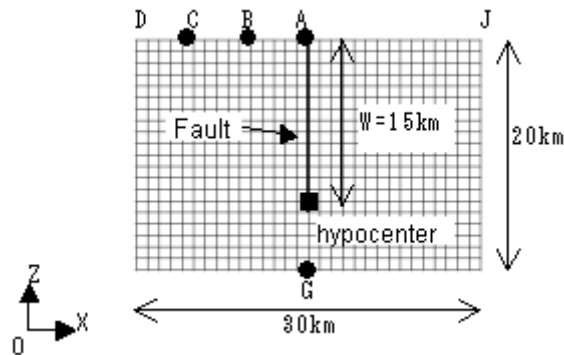


Figure-6 2D analysis model

EXAMINATION OF THE VALIDITY OF OUR ANALYSIS METHOD

In order to investigate whether the analysis method of this research is appropriate, we compared the result from our method with that from the past study, i.e., the dislocation obtained by the method proposed by Day for strike slip fault. Using the same mesh size as shown in Figure-3, and the physical properties, the model with 20km long and 10km wide, as shown in Figure-7 was analyzed. The magnitude of the stress drop, $\Delta\tau$, was 3.5MPa and uniform on the fault plane. According to Day, the amount of dislocation, U , at point (y,z) is given by the following equation(6) for the aspect ratio $L/W = 2$. Where μ is the shear modulus.

$$U = \frac{\Delta\tau}{\mu} W \left[1 - \left(\frac{2z}{W} \right)^2 \right]^{\frac{1}{2}} (2 - \xi)^{\frac{1}{2}} \xi^{\frac{1}{2}} \quad (6)$$

$$\xi(y) = \begin{cases} \frac{|L-2y|}{W} & \text{if } |L-2y| < W \\ 1 & \text{if } |L-2y| \geq W \end{cases}$$

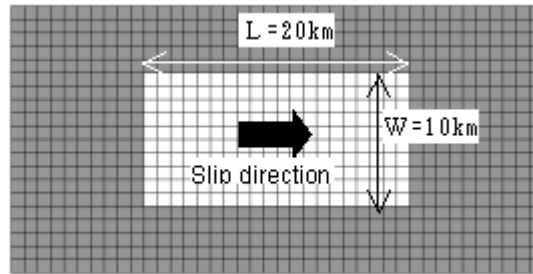


Figure-7 The fault plane of the model used for the comparison with the Day's method

Figure-8(a) shows the distribution of the dislocation which was obtained from equation (6) and Figure-8(b) shows that obtained from our method. Although the dislocation is produced within the Y-Z plane, it is illustrated perpendicular to the Y-Z plane in order to make it luminous. Table-2 summarizes the maximum dislocation and the average dislocation for each method. Although the distribution by Day's is constant around the center of the fault as clear from equation (6), the distribution by our analysis method is convex around the center as shown in Figure-8(b). About 5% of difference has arisen in maximum values and about 3% of difference for average values. Although the distribution forms looks a little different, the magnitudes of dislocations are almost same, and this shows the validity of our method.

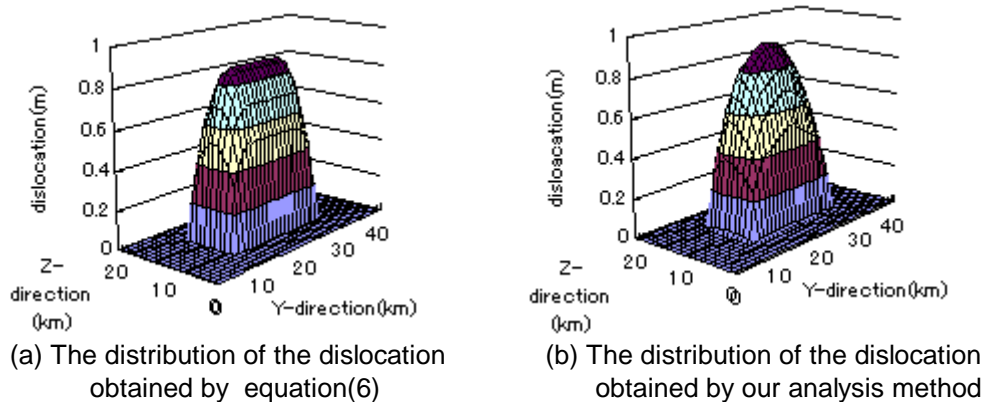


Figure-8 Comparison of the distribution of the dislocation

Table-2 Comparison of obtained dislocations

	Maximum dislocation	Average dislocation
Our method I	0.92m	0.64m
Equation (6) II	0.88m	0.62m
I / II	1.05	1.03

ANALYSIS RESULTS

By keeping the fault width, W , an angle of inclination, δ , of the fault, and stress drop $\Delta\tau$, and changing the fault length, we investigated the effect of the fault length on the dislocation, seismic waves and so forth. The length of 16km, 22km, 30km, and 45km and the width of 15km are assumed so that the ratios of the width to the length, $W:L$ are 1:1, about 1:1.5, 1:2, and 1:3. In case4 with a fault length of 45km, the length of the Y direction was increased by 1.5 times due to the capacity of our computer. The size of the model is 30km in X direction, 60km in Y direction, and 20km in Z direction, and the element for the crust is $1\text{km} \times 1.5\text{km} \times 1\text{km}$ rectangular parallelepiped. The initial shear stress is given only in the Z direction for all joint elements ($\lambda = 90$ degrees).

The distribution of the dislocation

The distributions of the dislocation along the fault are shown in Figure-9. Although the center ($Y=20\text{km}$) of the distribution is keenly sharp in Figure-9(a), it becomes gently sloping as the length of the fault increases. The maximum dislocation in Figure-9(d) is about 2.4m, and we can see that the magnitude will saturate as the length of the fault increases.

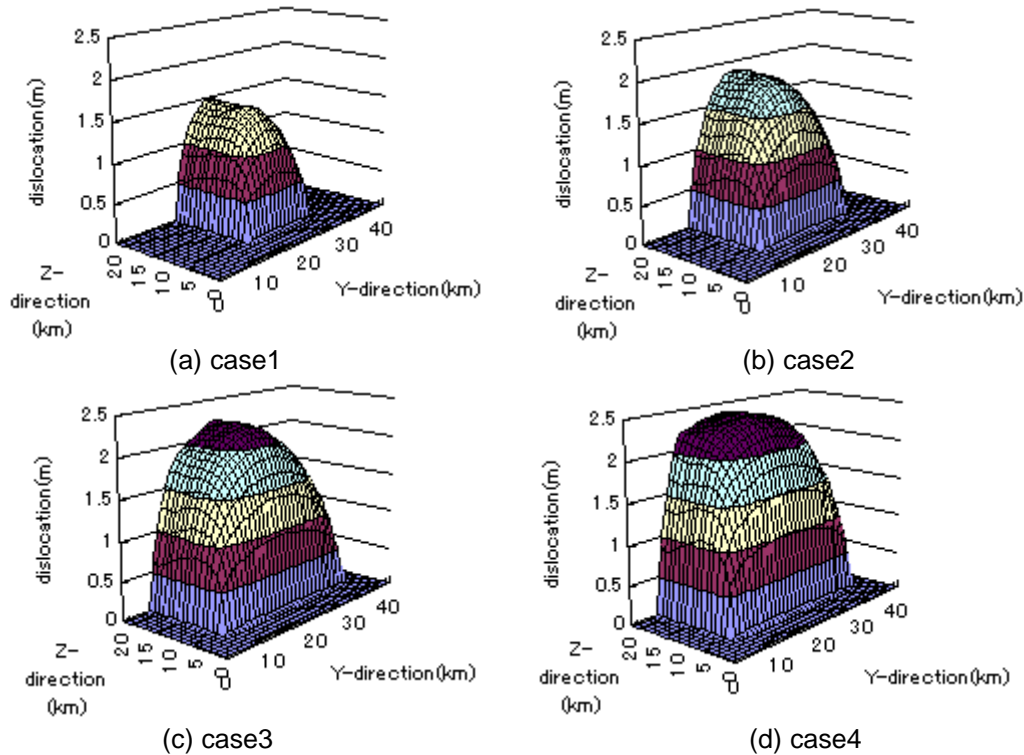


Figure-9 The distribution of the dislocation of the fault plane

Permanent displacement on the ground surface

Considering the aseismic design of structures near a fault, it is very important to know the magnitude and the shape of the residual displacement of the ground surface as well as ground motions. Although it is difficult to obtain the shape of the ground surface by conventional analysis techniques, it is possible for our technique. Figure-10 shows the distributions of the vertical displacements at the ground surface after ceasing the rupture.

As the initial stress component is in the vertical direction, the direction of the dislocation is so-called dip slip. Since the fault plane is vertical, the shape of the displacement is conversely symmetrical about the fault plane. From Figure-10, we can see that when the fault length is short, the distribution will appear in the central part of the fault intensively. But it becomes gently sloping as the fault length increases. In case4, around the central part of the fault, the displacements are almost constant.

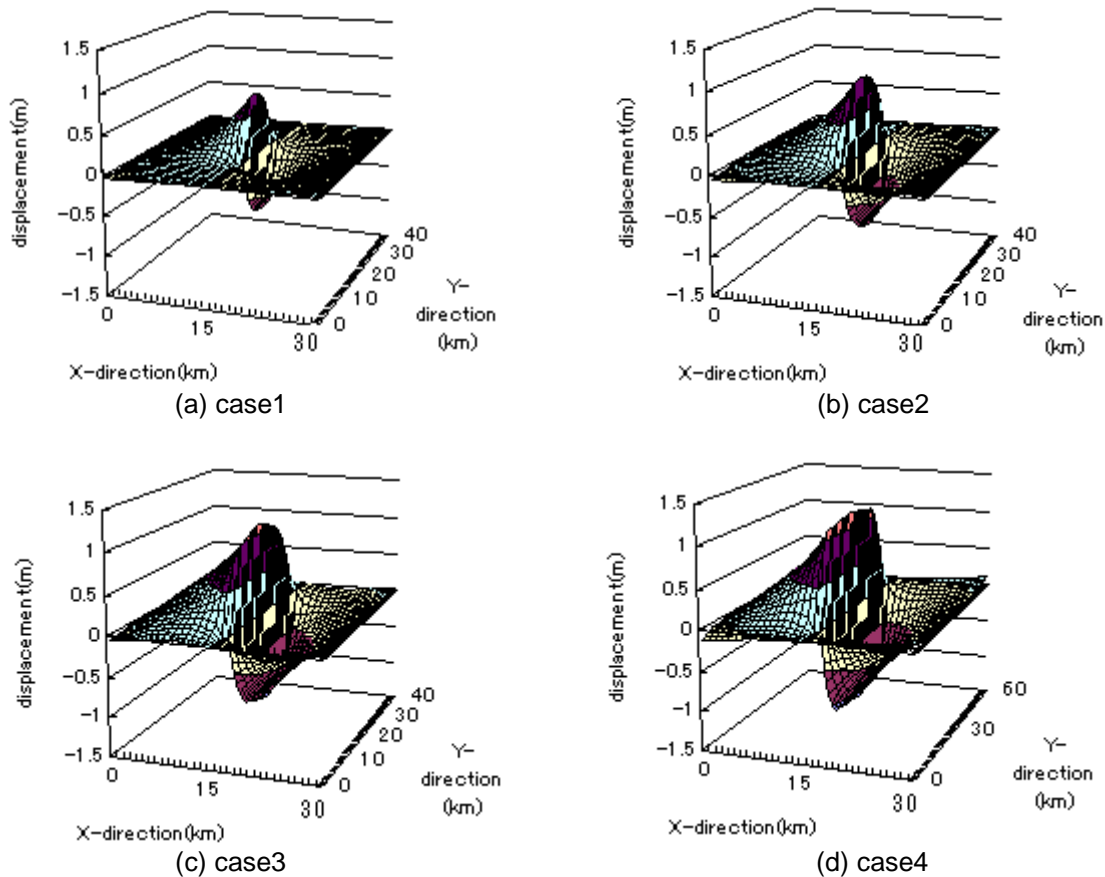


Figure-10 Distribution of the vertical residual displacements on the ground surface

Comparison of the magnitude of dislocations

The average dislocations obtained from 3D-FEM and 2D-FEM are listed in Table-3. In this table, “average” means the average of the dislocation for the whole fault plane, and “center” means the average dislocation on the central line of the fault plane (the A-G line except non-rupture zone in Figure-3).

Table-3 Comparison of the average dislocations (unit:m)

3D analysis	"average" dislocation	"center" dislocation
Case1	1.13(43.6)	1.39(54.1)
Case2	1.40(54.4)	1.73(67.3)
Case3	1.64(63.8)	2.01(78.2)
Case4	1.88(73.2)	2.16(84.1)
2D analysis	—	2.57

The values in () are % of the 3D/2D

The dislocation from 2D analysis is 2.57m as shown in Table-3. All the dislocations obtained from 3D analyses are smaller than that from 2D analysis, and when the fault length of 3D analysis becomes long, the magnitude approaches to 2D magnitude. Only the lower end of the fault is restrained in 2D analysis, in addition to it, the both side ends of the fault plane are also restrained in 3D analysis. This is why when the fault length is short, the restraint of these both sides works and the difference between the two becomes large.

The 2D analysis result is about 128% of that in case3, about 119% of that in case4 for the average dislocations at the "center" of 3D analysis. In other words, when width : length is 1:2, and when it is 1:3, the magnitude of dislocation from 2D analysis is about 20% and about 30% larger than that from 3D analysis, respectively.

Figure-11 shows the distribution of the dislocation on the fault vertical central line. The forms of the distribution are similar and this implies that it is possible to predict the distribution of 3D analysis result from the distribution of 2D analysis result. Then, we obtained the regression equation which represents the relationship between the ratio of the 3D and 2D results (3D/2D) and the ratio of the fault length and the fault width (L/W). By employing the boundary conditions of 3D/2D=0 at L/W=0, and 3D/2D=∞ at L/W=1, the regression curve is expressed by equation(7). The relationships are shown in Figure-12.

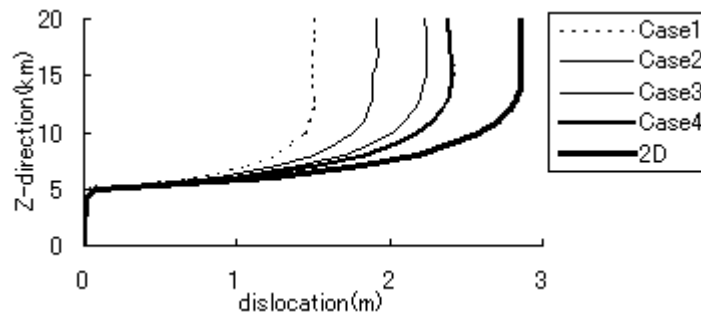


Figure-11 Comparison of distributions of dislocations in fault vertical center line

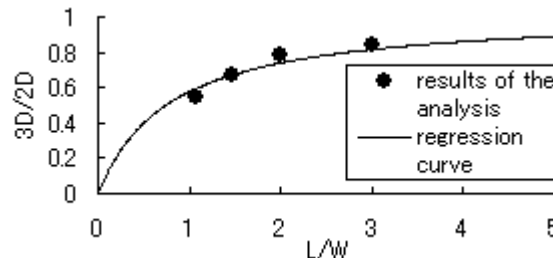


Figure-12 The relationship between 3D/2D and L/W and the resultant regression curve

$$3D/2D = -\frac{0.803}{L/W + 0.777} + 1.029 \quad (7)$$

Like this equation, if the condition of the analysis is similar, it will be thought that there is a possibility of presuming the average dislocation of 3D analysis result from that of 2D analysis result. Since this dislocation is directly related to the shape of the ground surface, when considering an earthquake-proof design of structures, it can be expected that the relation of equation (7) offers useful information.

Comparison of waveforms

In comparing waveforms, filter processing is necessary to compare seismic waves based on the same frequency range. Let f_0 be the frequency of the wave, the following relation can be obtained.

$$f_0 = \frac{V}{n \times l} \quad (8)$$

Where V is the shear wave velocity, n is the number of elements per 1 wavelength, l is the length of an element. According to the results from 2D analysis, if we employ the number of elements per wavelength equals to more than four, i.e., $n \geq 4$, there will be no change in a waveform [9]. So $n = 4$ is adopted here, and $l = 1\text{km}$, $V = 4.0\text{ km/s}$ are substituted to equation (8), and frequency $f_0 = 1.0\text{Hz}$ was obtained. Therefore, all the waveforms here after are filtered by 1.0Hz low path filter.

Comparison of the waveform of 3D analyses

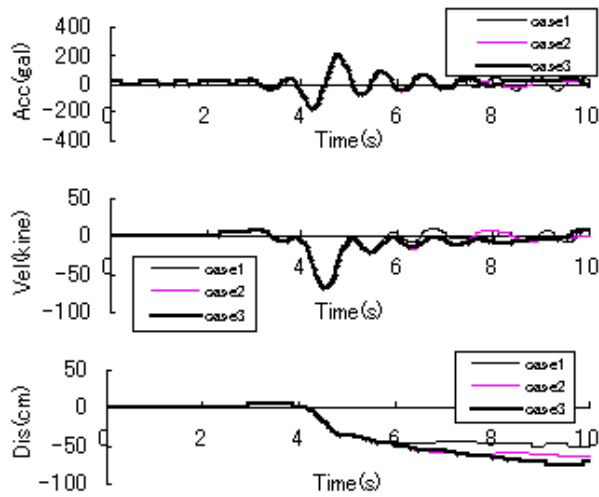
The acceleration, velocity, and displacement waveforms from case1 to case3 were compared. The points where waves were obtained are A, B and C shown in Figure-3 and Figure-6. Although, in 3D analyses, three components of X, Y and Z were computed, only X and Z components were compared since this analysis was dip slip and the wave of Y component was zero. The waveforms at A, B, and C points are shown in Figure-13, Figure-14, and Figure-15, respectively. The time of the horizontal axis is the lapsed time after the beginning of the analysis.

At point A, acceleration and velocity waveforms are completely in good agreement till about 5.0 seconds, and no large difference can be observed in the subsequent time. Displacement waveforms are also completely in good agreement till 5.0 seconds, however, after that the difference appeared, since the residual displacement became large as fault length became large. At points B and C acceleration and velocity waveforms are also in good agreement till around 4.5 seconds with the same tendency as point A. However, even point A, there is a large difference in displacement waveform after about 5.5 seconds.

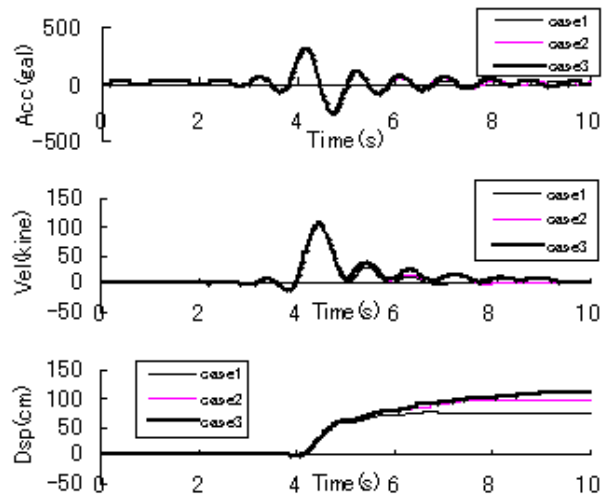
Comparison of waveforms with 2D analysis result

The waveforms of 3D and 2D analysis results were compared. The waveforms in case3 are used in comparison with 2D results. Waveforms are shown in Figure-16, Figure-17 and Figure-18. Figure-16 is at point A, Figure-17 is at point B, and Figure-18 is at point C. The time of the horizontal axis is the lapsed time after the 2D analysis starts. The waveforms of 3D analyses are shifted by 1.7 seconds late so that the phase in early stages of the waveforms of 2D analysis may overlap. The difference of 1.7 second is related to the difference of the rupture propagation.

Right above the fault shown in Figure-16, point A, there is no so large difference and they are comparatively well alike. About the waveforms of displacement, as for the maximum of 3D analysis, X and Z components have become about 80% of 2D analysis. This ratios are almost same as those about the ratio of the dislocation of 2D analysis result and the central dislocation of 3D analysis result.

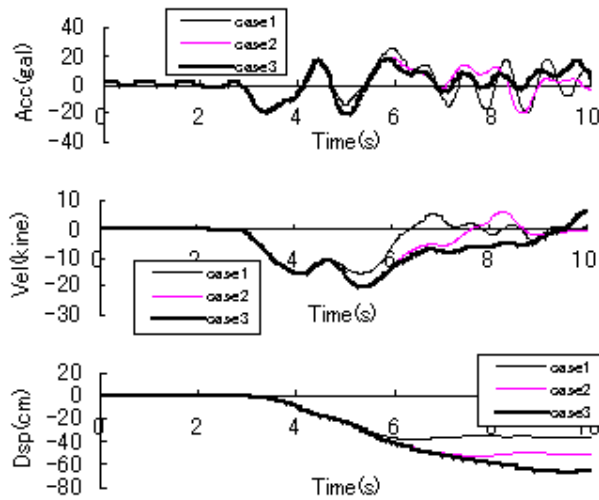


(a) X component

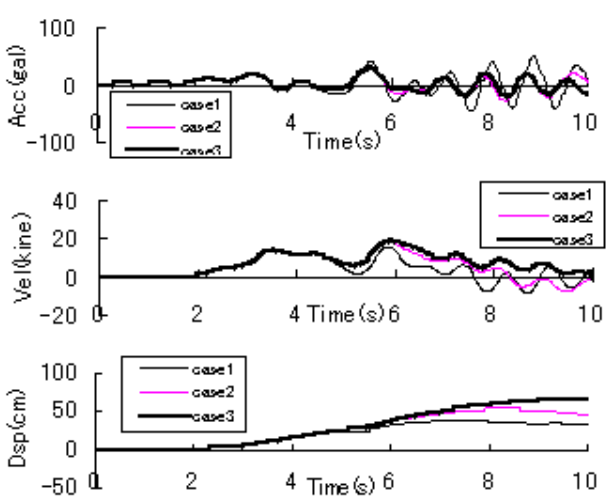


(b) Z component

Figure-13 Waveforms at point A (Acceleration, Velocity, Displacement from the top)

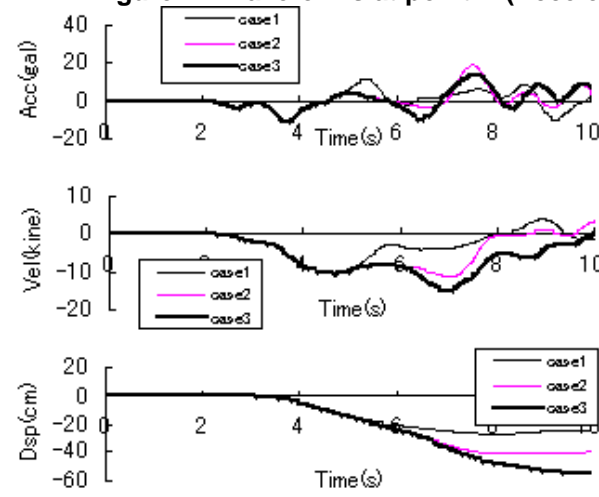


(a) X component

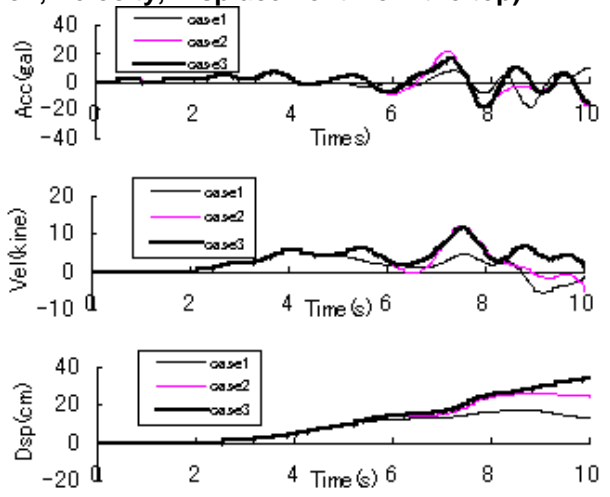


(b) Z component

Figure-14 Waveforms at point B (Acceleration, Velocity, Displacement from the top)

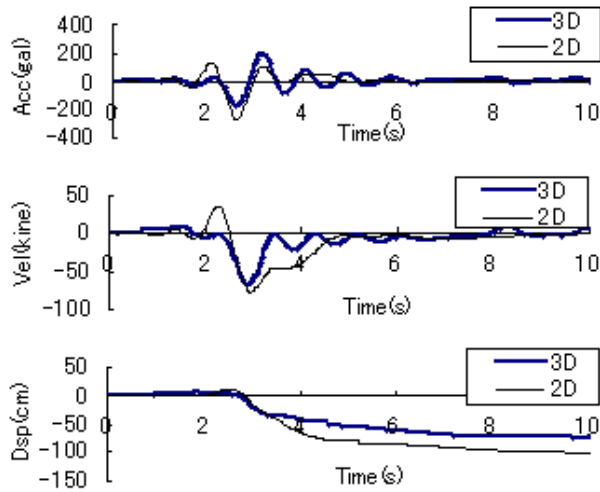


(a) X component

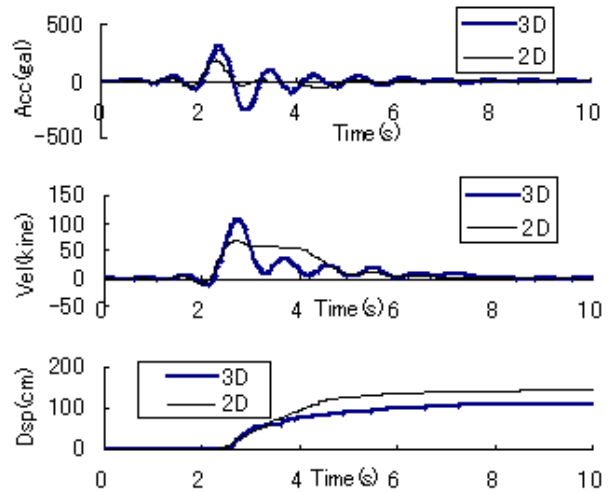


(b) Z component

Figure-15 Waveforms at point C (Acceleration, Velocity, Displacement from the top)

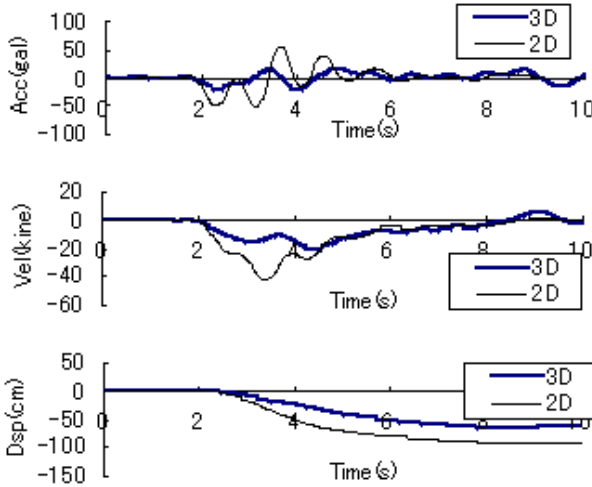


(a) X component

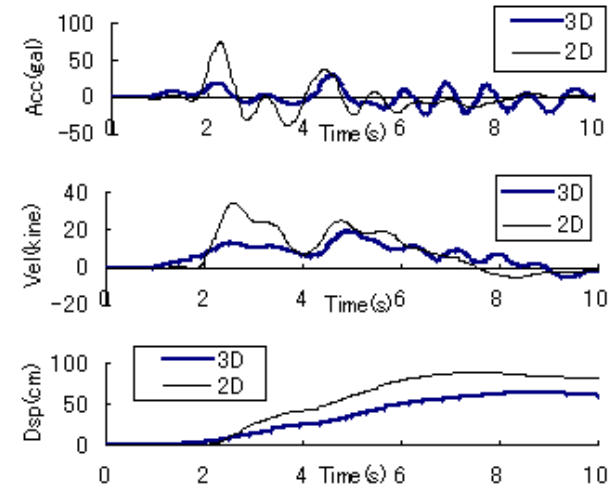


(b) Z component

Figure-16 Waveforms at point A (Acceleration, Velocity, Displacement from the top)

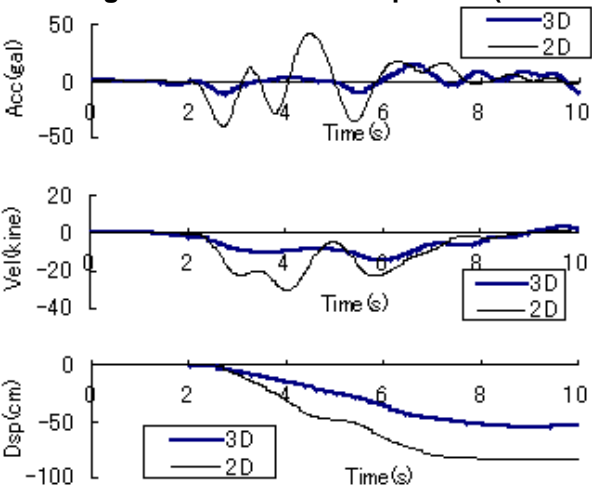


(a) X component

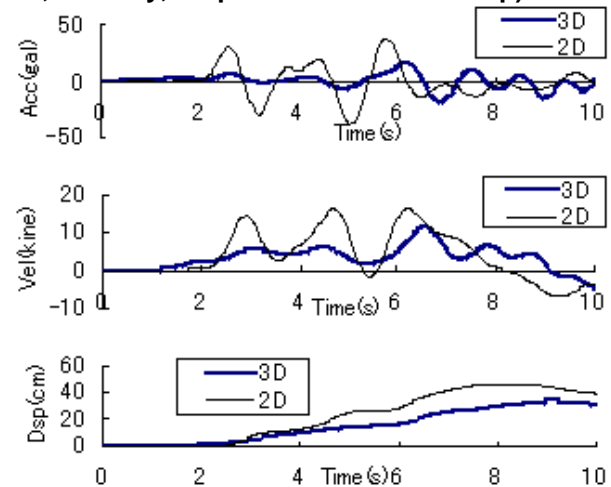


(b) Z component

Figure-17 Waveforms at point B (Acceleration, Velocity, Displacement from the top)



(a) X component



(b) Z component

Figure-18 Waveforms at point C (Acceleration, Velocity, Displacement from the top)

Difference appears notably and comparison is no longer difficult on points B and C where are far from the fault. On the waveforms of displacements, the maximum value of 3D analysis has become about 80% of 2D analysis. As mentioned above, it becomes impossible to see the resemblance as the observed point separates from the fault, although the forms of waves resemble to the 2D analysis result comparatively right above the fault. It is because the rupture propagation in 3D analyses differs from 2D analysis, that is, 3D analysis has the point source, while 2D analysis has the line source.

CONCLUSIONS

Fault rupture simulations were performed using 3D-FEM, by changing the fault length, and the dislocation of the fault, residual ground displacement, and the difference in waveforms of earthquake motion were investigated in this paper. Also by performing 2D analyses, comparing between both results were made. The obtained results are summarized below.

1. Comparison with the dislocation by the method proposed by Day was made, and these was a good agreement between the results from Day and from our method, which shows the validity of our method.
2. The average magnitude of dislocation becomes large and approaches to the 2D result as the fault length increases. The relationship between the dislocations from the 3D and those from the 2D analyses was expressed as a function of the ratio of the length of the fault and the width of it.
3. In the comparison of waveforms, the amplitude and the phase of the waves from 3D analyses and from 2D analyses correspond well when the observed point is on the fault. However, the difference between them from the 3D and 2D analyses increases if the distance from the fault becomes large.

REFERENCES

1. The 1999 Taiwan Chi-Chi Earthquake disaster investigation report and emergency restoration technology, Architectural Institute of Japan, 2000. (In Japanese)
2. Highway bridge specifications and descriptions, V, earthquake-proof design, Japan Road Association, p.11, 2002. (In Japanese)
3. Proceedings on the workshop for the earthquake resistant design of pile foundations, Japan Society of Civil Engineers, p.302, 2001. (In Japanese)
4. Toki, K. and Miura, F. : Simulation of a fault rupture mechanism by a two-dimensional finite element method, *J.Phys.Earth*, Vol.33, pp.485-511, 1985.
5. Steven M. Day : Three-dimensional finite difference simulation of fault dynamics : Rectangular faults with fixed rupture velocity, *BSSA*, Vol.72, No.3, pp.705-727, 1982.
6. Miura, F., Okasige, Y. and Okinaka, H. : Analysis of the rupture propagation using the 3D joint element, Research Report of Faculty of Engineering, Yamaguchi University, Vol.36, No.1, pp.81-87, 1985. (In Japanese)
7. Miura, F. and Okinaka, H. : The dynamic analysis technique of the 3D structure-foundation system using the viscous boundary based on the principle of virtual work, *JSCE Journal*, No.404/I-11, pp.395-404, 1989. (In Japanese)
8. Reconnaissance Report on the Northridge, California, Earthquake of July 17, 1994, Japan Society of Civil Engineers, 1997. (In Japanese)
9. Mizumoto, T., Miura, F. and Tsuboi, T. : Fundamental examination on analysis method of fault rupture model by FEM, Proceeding of the annual conference of the institute of social safety science, No.10, pp.189-192, 2000. (In Japanese)